1548 *KSME International Journal, Vol. 15 No. 11, pp. 1548~1554, 2001*

# Numerical Analysis of Ship's Propulsion Mechanism of Two-Stage Weis-Fogh Type by Discrete Vortex Method

**Ki-Deok Ro*, Soo Whan Ahn**

*School of Transport Vehicle Engineering · Institute of Marine Industry, Gyeongsang National University, Gyeongnam 650-160, Korea*

Flow patterns and dynamic properties of two-stage Weis-Fogh type ship propulsion mechanism are studied by a discrete vortex method. To study mutual interference between two wings, two cases are considered - wing motions with the same and reverse phases. The predicted flow patterns correspond to the available flow visualization results. Time histories of thrust and drag coefficients are also calculated, and the interference between the two wings are numerically clarified.

**Key Words :** Hydraulic Machine, Numerical Analysis, Unsteady Flow, Separation, Visualization, Fluid Force, Discrete Vortex Method, Ship Propulsion

## 1. Introduction

The Weis-Fogh mechanism (Weis-Fogh, 1973 and Lighthill, 1973) had been discovered by observing the hovering flight of small bees. Its higher efficiency and unique lift mechanism are attracting much attention (Maxworthy, 1979: Edwards, 1982: Spedding, 1986: and Ro, 1997). Vigorous attempts have been made to make use of this mechanism for engineering applications (Furber and Ffowcs Williams, 1979: Tsutahara and Kimura, 1987: Tsutahara, Kimura and Ro, 1989: Ro, 1993: Tsutahara and Kimura, 1987: and Tsutahara and Kimura, 1994).

Researchers proposed a Weis-Fogh type ship propulsion model. It has been shown that the proposed propulsion mechanism could be used as a new type of marine propulsion device (Tsutahara, Kimura and Ro, 1989). Moreover, unsteady flow fields were visualized (Ro, 1993), and time histories of thrust and drag coefficients of the wing were identified (Ro, 2000).

However, the propulsion mechanism also has propulsive power fluctuations and limitations in performance enhancement. Therefore, in this study, fluid dynamic characteristics, especially the effects of mutual interference between the two wings, will be identified for a 2-stage extended propulsion mechanism.

* Corresponding Author,
**E-mail** : rokid@gshp.gsnu.ac.kr
**TEL** : +82-55-640-3123; **FAX** : +82-55-640-3128
School of Transport Vehicle Engineering · Institute of Marine Industry, Gyeongsang National University, 445 Inpyeong, Tongyeong, Gyeongnam 650-160, Korea.
(Manuscript **Received** February 13, 2001; **Revised** September 12, 2001)

## 2. Calculation Method

### 2.1 Simulation of flow field

First, an analytical model of a 2-stage Weis-Fogh type ship propulsion mechanism is shown in Fig. 1. This is an extension of a 1-stage analytical model (Ro, 1993 and Ro, 2000). The wings are set as shown in the figure, the opening angle and the moving speed are the same for both wings, and the motion of each is as follows: A point p reciprocates in the channel along the dashed line. The wing with the trailing edge touching the side wall rotates (or opens up) up to an angle $\alpha$. The wing then translates keeping $\alpha$ constant. Once the leading edge touches the other wall the wing rotates or closes. The wings in Fig. 1 are to be referred to as ① and ②, the same phase means that two wings start to move at the

same surface, $\Delta T=0°$ while the reverse phase means that each of two wings starts to move at the opposite side of the water channel, $\Delta T=180°$. In theory, each wing is assumed to be a flat plated airfoil without thickness and is represented by equally placed bound vortices with numbers of m and m′ (m=m′=20 is used in this study). Assuming that the positions of the bound vortices of each wing correspond to $z_j$ and $z_j'$, and the positions of free vortices as $\bar{z}_l$ and $\bar{z}_l'$, the complex potential F(z) can be expressed as follows.

$$\begin{aligned}F(z)=&i\sum_{j=1}^{m}x_j\{\log\left\{\sinh\frac{\pi(z-z_j)}{2h}\right\}\\&-\log\left\{\sinh\frac{\pi(z-\bar{z}_j)}{2h}\right\}\}\\&+i\sum_{j=1}^{m'}x_j'\{\log\left\{\sinh\frac{\pi(z-z_j')}{2h}\right\}\\&-\log\left\{\sinh\frac{\pi(z-\bar{z}_j')}{2h}\right\}\}\\&+i\sum_{l=1}^{n}\bar{x}_l\{\log\left\{\sinh\frac{\pi(z-\bar{z}_l)}{2h}\right\}\\&-\log\left\{\sinh\frac{\pi(z-\bar{\bar{z}}_l)}{2h}\right\}\}\\&+i\sum_{l=1}^{n'}\bar{x}_l'\{\log\left\{\sinh\frac{\pi(z-\bar{z}_l')}{2h}\right\}\\&-\log\left\{\sinh\frac{\pi(z-\bar{\bar{z}}_l')}{2h}\right\}\}-Uz\end{aligned}\qquad(1)$$

In Eq.(1), h and U are the channel width and the uniform flow velocity; $x_j(j=1, 2 \ldots\ldots m)$ and $x_j'$ represent strengths of the bounded vortices; and $\bar{x}_l(l=1, 2\ldots\ldots n)$ and $\bar{x}_l'$ represent those of free vortices, respectively. Using conditions of the stream function and velocity, and Kelvin's theorem in the boundary conditions, we could determine the strengths of the vortices by taking the center point of the adjacent bounded vortices as a control point (Ro, 1993: Ro, 2000).

On the other hand, free vortices are generated at a location $\Delta C$ away from the trailing edge of the wing at each time step $\Delta t$. The following Euler's equations were applied for calculation for the motion of the $l$th free vortex, $\bar{z}_l$.

$$\bar{z}_l(t+\Delta t)=\bar{z}_l(t)+\overline{W}\cdot\Delta t\qquad(2)$$

$$W=\frac{d}{dz}\left[F(z)-i\bar{x}_l\log\left\{\sinh\frac{\pi(z-\bar{z}_l)}{2h}\right\}\right]$$

Here $W$ represents the complex velocity induced by total bound and free vortices in the flow field except $\bar{z}_l$.

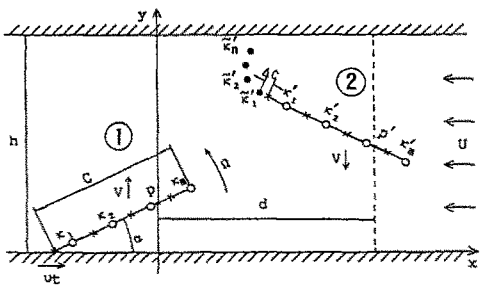


**Fig. 1** Model of the numerical analysis

To simlate the flow field, streaklines were calculated at every time step $\Delta t$ ($\Delta t=0.06$ is taken in this study) at a certain upstream location where tracers are introduced. To find the motion of each tracer circle, complex velocity is found from $W=dF/dz$(Eq.2). For timelines, tracer circles in a line perpendicular to the flow in upper stream generated at every constant time step ($7\times\Delta t$ is taken in this study), and the same was true with the streak lines in the motion method.

### 2.2 Force, moment and the coefficients of properties

Since calculation methods for force and moment are identical for both wings (① and ② in the Fig. 1), explanations is given only for Wing ①. Let $X$ and $Y$ represent the x and y components of the fluid force acting on the wing. They can be obtained by contour integration of the pressure around the wing surface as follows.

$$X-iY=\frac{i\rho}{2}\oint_B\left(\frac{dF}{dz}\right)^2dz+i\rho\oint_B\frac{\partial\bar{F}}{\partial t}d\bar{z}\qquad(3)$$

where $\rho$ represents the density of the fluid while B is the contour of integration along the wing surface. Also, $\coth\{\pi(z-z_j)/2h\}$ has its first extreme value at $z=z_j$, where the residue is $2h/\pi$. Therefore, the first term of the right hand side of the Eq. (3) can be easily obtained through the residue theorem. The second term on the right hand side of Eq. (3) can be evaluated according to Tsutahara, Kimura and Ro, 1989; and Ro, 2000. The wing surface is assumed to be the collective cuts of logarithmic singularities. The moment around point P in Fig. 1, $M_P$, can be calculated using the moment around the trailing

edge, $M_t$, and $X$, $Y$ from Eq. (3) as follows.

$$M_p = M_t + Im\{(X - iY)(z_p - z_t)\} \quad (4)$$

$$M_t = -Re\left\{\frac{\rho}{2}\oint_B \left(\frac{dF}{dz}\right)^2 (z - z_t)\, dz + e^{-2i\alpha}\rho \oint_B \frac{\partial \bar{F}}{\partial t}(\bar{z} - \bar{z}_t)\, d\bar{z}\right\}$$

Here $Im$ and $Re$ represent the imaginary and real components, respectively. Also $z_p$ is the position of point $P$, $z_t$ is the position of the trailing edge. The moment around the trailing edge of the wing, $M_t$, can be found in through a similar method. Then, if we assume the wing span to be of unit length, thrust coefficient, $C_T$ and drag coefficient, $C_D$ can be calculated as follows (Ro, 2000).

$$C_T = \frac{X}{\frac{1}{2}\rho V^2 C} \quad (5)$$

$$C_D = \frac{-Y + Y_W}{\frac{1}{2}\rho V^2 C} \quad (6)$$

## 3. Visualization Experiment Device and Method

Figure 2 shows a schematic of the wing driving unit. A visualization experiment was done with hydrogen in a circulating water tank (Ro, 1993). The chord of each wing, which determines the scale of the system, was set to 80mm. Also, the driving unit of wings is built for the wing to have the same motion as the analysis model described in Fig. 1. The power generated from the motor was relayed through a belt-pulley-worm gear-sprocket-chain system as shown in Fig. 2. The reciprocating motion of the slider was made possible by a pin on the upper part of the chain. The wing opens by the moment applied around the wing axis during the reciprocating motion of the sliders. An adjustable angle plate was installed on the upper part of the slider to maintain constant opening angle of the wing. The velocities of uniform flow, U, and wing, V, were controlled by variable motor speed. On the other hand, the cathode on the upper stream of the circulating water tank generated hydrogen bubbles in a dark room, and they were illumination through a slit from a slide projector (150W×3units) for visualization. The channel and wings in the experimental unit were built with transparent acrylic plates for optical access.

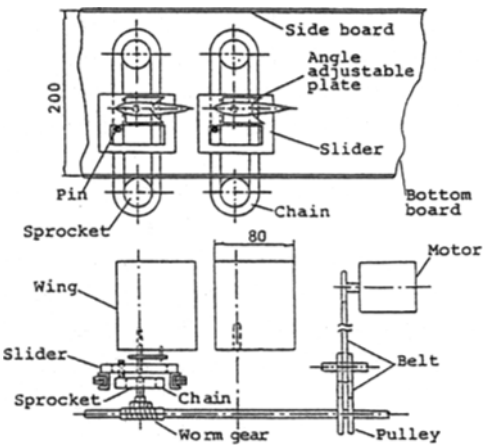


**Fig. 2** Driving system of wings (unit: mm)

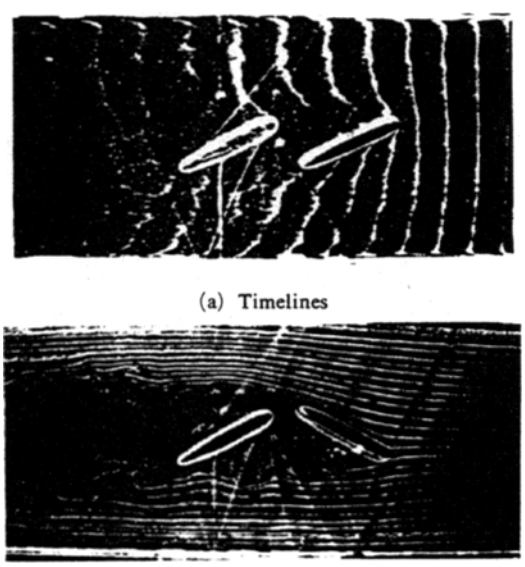

(a) Timelines

(b) Streaklines

**Fig. 3** Timelines and streaklines for stationary wings

## 4. Results and Discussion

### 4.1 The flow pattern around the wing

To fully understand the flow patterns around the two wings, we analysed the continuous flow pattern around the wings during one stroke and compared it to the visualized photograph. An

opening angle of 30°; a water channel width of 2.5C; velocity ratio of the wing and the uniform flow vcloity of 1.0; the distance between the two wings of 1.15C; and the distance from the trailing edge of the wing to the wing axis of $0.75C$ were assumed.

The photographs of timelines and streaklines around wings are shown in Fig. 3. In this case, the two wings are stationary in a uniform flow of $U=8cm/sec$, corresponding to a Reynolds number of 5,900. The uniform flow proceeds from right to left. In Figs. 3(a) and (b), separation occurs from the leading and trailing edges of the front wing, and the separation region covers the entire area of the rear wing. However, in Figs. 4 (a) and 5(a), no separation occurs at the leading edge of the wing and the streaklines on the back side of the entire wing are clearly visible.

Figures 4 and 5 show the visualized photographs and predicted results when two wings move toward the center of the water channel in the same and the reverse phases, respectively. The flow patterns show a fairly good match in qualitative trends, validating the effectiveness of the proposed simulation method.

The continuous flow pattern around the wing during a stroke in the same phase is shown in Fig. 6. In this case, 1 represents the opening stage, 2 to 4 the translating stages and 5 the closing stage, respectively. The figures show simultaneous streaklines and timelines. The streaklines passing the wing during the entire process are bent in the direction of the wing motion, and this change in direction is affected by both front and rear wings and the channel. This implies that the two wings interfere with each other during the entire process. Also, from a careful observation of the inclination of timelines passing through each wing, the flows on the pressure surfaces of the two wings are accelerated. Also the cirulations around both wings are in the same direction (clockwise).

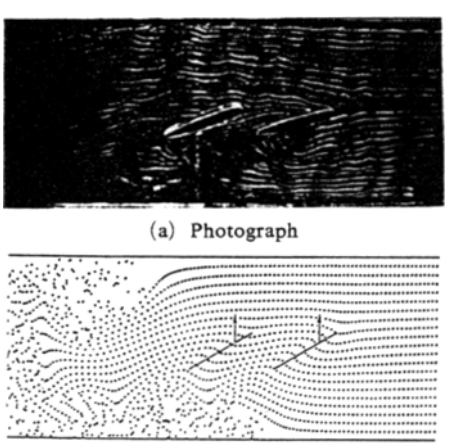

(a) Photograph

(b) Simulation

**Fig. 4** Streaklines for the same phase

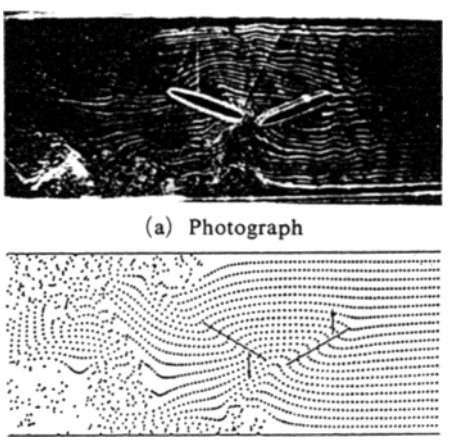

(a) Photograph

**Fig. 5** Streaklines for the reverse phase

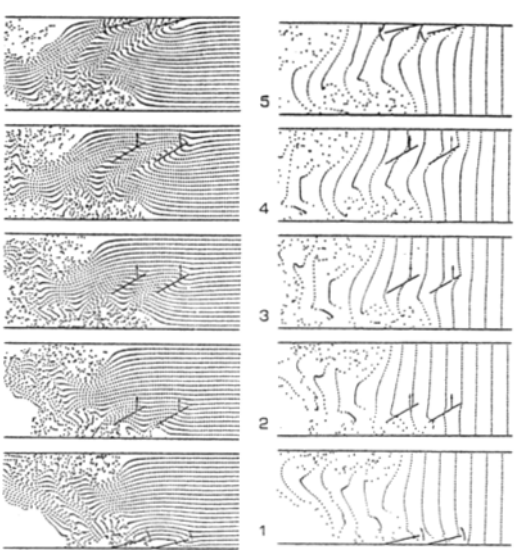


**Fig. 6** Streaklines and timelines for the same phase through a stroke

Thrust force occurs at each wing in the opposite direction to the uniform flow. Moreover, a downstream recirculation zone forms near each side of the channel, like that in a 1-stage propulsion mechanism (Ro, 2000), and it moves along with the uniform flow toward the downstream.

Figure 7 shows the flow pattern with identical conditions as that in Fig. 6 except for the reverse phase. Discontinuous streaklines inclined in the direction of the channel sides at the trailing edge of the wing can be found. This might be attributed to the effect of free vortices generated at the trailing edge of the wing in the motion. From frames 3 and 4 show that, due to the bent direction of time lines passing the wing, the flow on the pressure surface is accelerated after the two wings go past each other, and counter-clockwise and clockwise direction circulations exist on the front and rear wings, respectively. Therefore, thrust force on each wing acts in the opposite direction to the uniform flow as described in Fig. 6. Also, turbulent flows can be found near each side of the channel near down stream.

### 4.2 Dynamic properties

Dynamic properties, particularly the effects of mutual interference between the two wings, are identified by calculating the time variation of thrust and drag coefficients. The distance and the phase difference of motion between the two wings were considered the variables.

Figure 8 shows the calculated results of the thrust coefficient, $C_T$, and the drag coefficient, $C_D$, when the distance between the two wings, d, equals 2C in the same phase. The horizontal axis representing the moved distance of a wing divided by the channel width corresponds to the number of the strokes.

Almost no difference in the values of the thrust and drag coefficients on front and rear wings are almost identical, as they are in a 1-stage system (Ro, 2000). This means that no interference between the wings occurs as the wings move far away from each other.

Figure 9 shows the predicted results of the thrust coefficient, $C_T$ and the drag coefficient, $C_D$ for the same conditions as those in Fig. 8 except for the distance between the two wings, which is 1.1C. Smaller distance between the wings always leads to more interference during a stroke and larger coefficients on the front wing. Moreover, comparing Figs. 8 and 9, both coefficients increase on the front wing, while they decrease on the rear wing. The average values of each

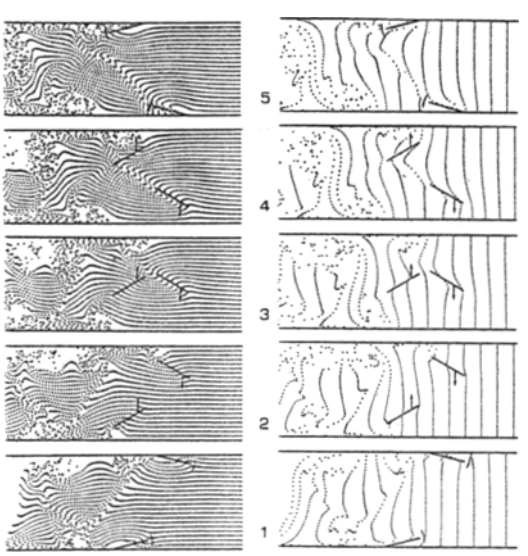


(a) Streaklines (b) Timelines

**Fig. 7** Streaklines and timelines for the reverse phase through a stroke

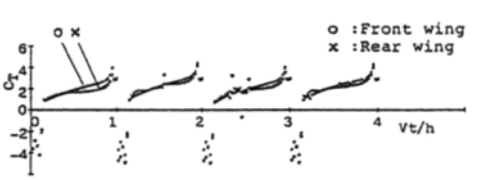


(a) Thrust coefficient

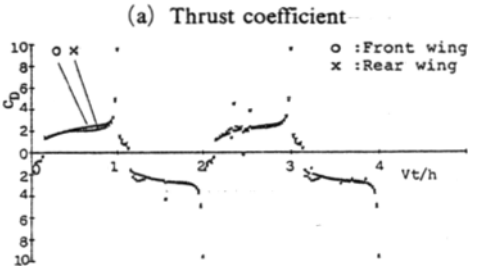


(b) Drag coefficient

**Fig. 8** Thrust and drag coefficients in the same phase and the distance d=2C

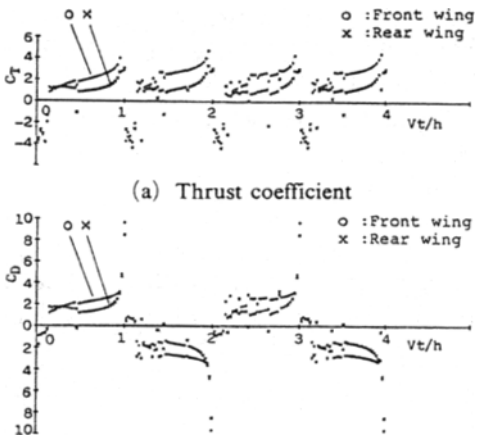


(a) Thrust coefficient

(b) Drag coefficient

**Fig. 9** Thrust and drag coefficients in the same phase and the distance d=1.1C

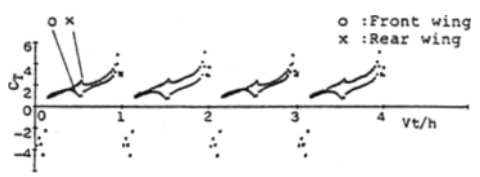


**Fig. 10** Thrust coefficient in the reverse phase and the distance d=1.1C

coefficient on the two wings are the same as the 1-stage propulsion mechanism (Ro, 2000).

Figure 10 shows the calculated results of the thrust coefficient $C_T$ for the reverse phase for the same conditions. The interference between the two wings is more significant as the two wings get closer in the central region of the channel. In addition, contrary to the characteristics of the same phase, as the two wings get closer, the value of the thrust coefficient at the front wing decreases while that of the rear wing increases. However, the average value of the coefficient on the two wings is the same as that of the thrust coefficient in the same phase. The reason for the difference in the mutual interference between the same and the reverse phases can be explained from the circulation around the wing.

Figure 11 represents the direction of the circulation around each wing when the positive thrust force in the opposite direction to the uniform flow is applied. As shown in Fig. 11(a), the directions

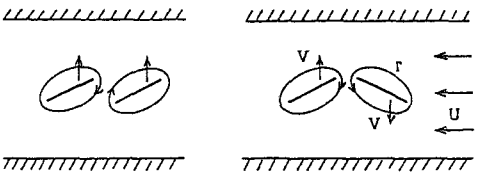


(a) Same phase (b) Reverse phase

**Fig. 11** Circulations about two wings

of the circulations in the region between the wings are opposite to each other when they are in the same phase, which results in slower flow and higher pressure. Accordingly, each coefficient value on the front wing increases, while it decreases on the rear wing. In the reverse phase, shown in Fig. 11(b), the circulation of opposite direction exists on each wing. Therefore, when the two wings get closer, the flow velocity increases and the pressure decreases in the region. The pressure drop leads to the decrease of the thrust force on the front wing and the increase on the rear wing.

## 5. Conclusion

The characteristics of the flow field for a 2-stage Weis-Fogh type ship propulsion mechanism were analyzed by numerical calculation using a discrete vortex method. The predicted results matched fairly with the flow visualization data. In addition, the effects of the mutual interference between two wings were identified by calculating the time histories of thrust and drag coefficients acting on the wing. The results can be summarized as below.

(1) Separation occurs at the leading and trailing edges of the front wing when the wing remains stationary, while no separation occurs when the wing moves in a direction perpendicular to the flow.

(2) The flow on the pressure surface of the wing is accelerated when the wing is in a translational motion.

(3) The interference between two wings always occurs when motion takes place in phase. Thrust coefficient as well as drag coefficient increase on the front wing and decrease on the

rear wing.

(4) The interference is more significant as two wings get closer when motion takes place out of phase. Thrust coefficient decreases on the front wing, and increases at the rear wing.

(5) The direction of circulation around each wing can be analyzed from the timelines passing through the wing, and the characteristics of mutual interference between the two wings in each phase can be explained from the circulation direction.

## Acknowledgement

This work was supported by Brain Korea 21 Project.

## References

Edwards, R. H. and Cheng, H. K., 1982, "The Separation Vortex in the Weis-Fogh Circulation -Generation Mechanism," *Journal of Fluid Mechanics*, Vol. 120, pp. 463~473.

Furber, S. B. and Ffowcs Williams, J. E., 1979, "Is the Weis-Fogh Principle Exploitable in Turbomachinary ? ," *Journal of Fluid Mechanics*, Vol. 94, Part 3, pp. 519~540.

Lighthill, M. J., 1973, "On the Weis-Fogh Mechanism of Lift Generation," *Journal of Fluid Mechanics*, Vol. 60, Part 1, pp. 1~17.

Maxworthy, T., 1979, "Experiments on the Weis-Fogh Mechanism of Lift Generation by Insects in Hovering Flight. Part 1. Dynamics of the 'Fling'," *Journal of Fluid Mechanics*, Vol. 93, pp. 47~63.

Ro, K. D. and Tsutahara. M., 1997, "Numerical Analysis of Unsteady Flow in the Weis-Fogh Mechanism by the 3D Discrete Vortex Method with GRAPE3A," *Transactions of the ASME, Journal of Fluids Engineering*, Vol. 119, pp. 96~102.

Ro, K. D., 1993, "Development of the Weis-Fogh Type Ship Propulsion Mechanism (Visualization and Numerical Analysis of the Flow Field)," *Transactions of the KSME*, Vol. 17, No. 2, pp. 426~437 in Korean.

Ro, K. D., 2000, "Calculation of Thrust and Drag Characteristics for Ship's Propulsion Mechanism of Weis-Fogh Type," *KSME International Journal*. Vol. 14, No. 11, pp. 1257~1266.

Spedding, G. R. and Maxworthy, T., 1986, "The Generation of Circulation and Lift in a Rigid Two-Dimensional Fling," *Journal of Fluid Mechanics*, Vol. 165, pp. 247~272.

Tsutahara, M. and Kimura, T., 1987, "An Application of the Weis-Fogh Mechanism to Ship Propulsion," *Transactions of the ASME, Journal of Fluids Engineering*, Vol. 109, pp. 107~113.

Tsutahara, M., Kimura, T. and Ro, K. D., 1989, "Ship Propulsion Using the Weis-Fogh Mechanism," *Bulletin of the Marine Engr. Soc. in Japan*, Vol. 17, No. 2, pp. 49~55.

Tsutahara, M. and Kimura, T., 1987, "A Pilot Pump using the Weis-Fogh Mechansm and its Characteristics," *Transactions of the JSME*, Vol. 54, No. 498, pp. 393~397.

Tsutahara, M. and Kimura, T., 1994, "Study of a Fan Using the Weis-Fogh Mechanism (An Experimental Fan and Its Characteristics)," *Transactions of the JSME*, Vol. 60, No. 571, pp. 910~915.

Tsutahara, M., Kimura, T. and Ro, K. D., 1989, "Unsteady Pressure and Force in the Discrete Vortex Methods," *Transactions of the Japan Soc. Aero. Space Sci*. Vol. 32, No. 97, pp. 129~142.

Weis-Fogh, T., 1973, "Quick Estimates of Flight Fitness in Hovering Animals, Including Novel Mechanism for Lift Production," *Journal of Experimental Biology*, Vol. 59, pp. 169~230.